Vol. 12(3), pp. 47-56, July-September, 2020
DOI: 10.5897/IJWREE2015.0624
Article Number: 0860FAA64241
ISSN 2141-6613

http://www.academicjournals.org/IJWREE

ACADEMIC JOURNALS
expand your knowledge

International Journal of Water Resources and Environmental Engineering

*Full Length Research Paper*

# Influence of bed roughness on near-bed turbulent flow characteristics

**Ratul Das* and Sinan Nizar**

Department of Civil Engineering, National Institute of Technology, Agartala, 799055, Tripura, India.

Received 21 November, 2015; Accepted 15 August, 2018

**Influence of bed roughness on near-bed flow characteristics is of considerable importance, especially in turbulent flows over rough beds. This experimental study is devoted to insight various turbulent flow characteristics such as velocity distributions, Reynolds shear stresses (RSS) and velocity power spectra at the groove, lee and crest level of carrier fluid in an immobile gravel bed stream. Uniform round shape gravels were used in five layers in a laboratory flume. Nortek's *Vectrino* four-receiver Acoustic Doppler velocimeter (ADV) probe was used to capture the instantaneous three-dimensional velocity components at groove. The interference between incident and reflected pulses in the ADV data measured in the near-bed flow zone produced spikes. Spikes were detected and filtered with a spike removal algorithm based on the acceleration threshold method. The velocity power spectra provides a satisfactory fit with the Kolmogorov "–5/3 scaling-law" in the inertial subrange. Velocity distributions below the roughness crest level fairly follows a third-degree polynomial series.**

**Key words:** Bed roughness, gravel-bed stream, turbulence, Reynolds shear stresses, inertial sub-range.

## INTRODUCTION

In natural open channel turbulent flow the effect of bed roughness on different turbulent characteristics is a long standing topic of interest to the community of research and solid research is going on this topic (Sadeque et al., 2009; Reidenbach et al., 2010; Ibrahim and Abdel-Mageed, 2014; Pal and Ghoshal, 2014). Significant progress has so far been achieved in understanding the near-bed turbulence parameters over rough-bed flows by many researchers. Nikora et al. (2001) studied the turbulent flow characteristics over spherical elements as bed roughness. They showed that the streamwise velocity distribution follows a linear profile below the spherical crests. In another experimental study conducted by Mignot et al. (2009a) over a bed of angular crushed stones revealed that the Reynolds shear stress (RSS) reaches its maximum at the gravel crests. Sarkar and Dey (2010) studied the double average (DA) RSS of a gravel-bed and examined the pressure energy diffusion below the virtual bed level. Also, Dey and Das (2012) examined by applying DAM and found the velocity distribution within the inertial ranges deviated from logarithmic law and followed a polynomial series. Moreover, many investigations (Nikora et al., 2002a; Pokrajac et al., 2007; Manes et al., 2007; Franca et al., 2008; Nikora and Rowiński, 2008) studied flow characteristics on rough-bed flows and applied the

*Corresponding author. E-mail: ratulnitagrtala@gmail.com.

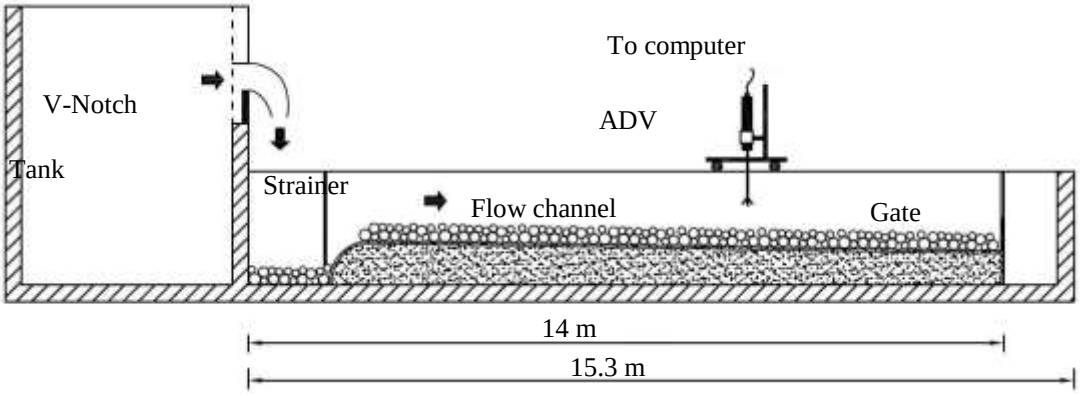


**Figure 1.** Schematic of the experimental setup.

Reynolds averaged Navier-Stokes equation for a steady flow over a rough-bed having zero-pressure gradient to determine total shear stress *τ* in the stream wise direction which can be expressed as:

$$\mu \frac{du}{dz} + -\rho \overline{u' w'}' = \tau_v + \tau_f = \tau \quad (1)$$

where, $\tau$ = total shear stress, $\tau_v$ = viscous shear stress, $\tau_f$ = turbulent shear stress, $-\rho\overline{u'w'}$ = Reynolds shear stress (RSS), $\mu$ = dynamic viscosity of fluid; and $z$ = elevation with respect to the roughness crests. But limited works so far been taken up to focus on the nature of velocity fluctuations at lowest bed level to the roughness crest and its influence on other turbulent flow characteristics such as velocity distribution, Reynolds shear stress and spectral density which is objective of the present study.

## Experimental setup and procedure

Experiments were conducted in the Water Resources Engineering Laboratory, Department of Civil Engineering, National Institute of Technology, Agartala. The dimension of the flume is 14 m length, 0.45 m width and 0.60 m deep. A schematic of the flume is shown in Figure 1. Uniform gravels of median size $d_{50}$ = 40 mm was laid homogeneously in five layers to simulate the turbulent flow. To achieve a uniform flow condition in the flume, the flow depth was controlled by gates at the downstream end of the flume. The experiment was run for a flow depth of 0.14 m (measured from the mean bed level) and a mean flow velocity of 0.21 m/s. The ADV was fitted for capturing velocity fluctuations sufficiently away from the downstream gate. The water was supplied to the flume from a tank having a total capacity of 3500 L. The tank was fed with two recirculation 5 HP mono-block pumps. The water from the overhead tank flows into the flume over a triangular notch having a notch angle of 60° with height 0.30 m and top width 0.35 m. The V-notch enables the measurement of quantity of water passing onto the flume. At the receiving end, the flume has a ditch packed with gravel to reduce the impact of falling water. The water then flows through the strainer which helps reduces the disturbances in the flow. The photograph of the flume with gravel bed is shown in Figure 2.

A 4-beam down looking Vectrino probe (Acoustic Doppler type) manufactured by Nortek was used to measure the instantaneous velocity components. It acted with an acoustic frequency of 10 MHz and a sampling rate of 100 Hz was set for the measurement. The measuring location was 5 cm below the probe. Thus the influence of the probe on the measured data was negligible. However, the limitation of the probe was that the measurement was not possible with in the flow zone 5 cm below the free surface. The sampling duration of 300 s was considered ensuring a statistically time independent average velocity. The data was collected along the centre line of the flume at a working section identified 9 m downstream of the inlet. The velocity fluctuations were recorded at the crest, lee and groove as shown in Figure 3.

## Despiking of ADV data

Acoustic Doppler Velocimeter (ADV) data have been extensively examined with a best combination of velocity threshold (VT) and acceleration threshold (AT) to ascertain near-bed turbulence parameters in the present study. In all experimental run, the signal-to-noise ratio and signal correlations between transmitted and received pulses were maintained 15 and 70% respectively as cut-off value. Data filtering with a spike removal algorithm based on the *acceleration threshold* method (Goring and Nikora, 2002) was performed. Figure 4(a, b) shows the typical mean stream wise velocity fluctuations measured with ADV before and after spike removal. The velocity threshold values for despiking were considered (by trial

**Figure 2.** Photograph of the flume with gravel bed.

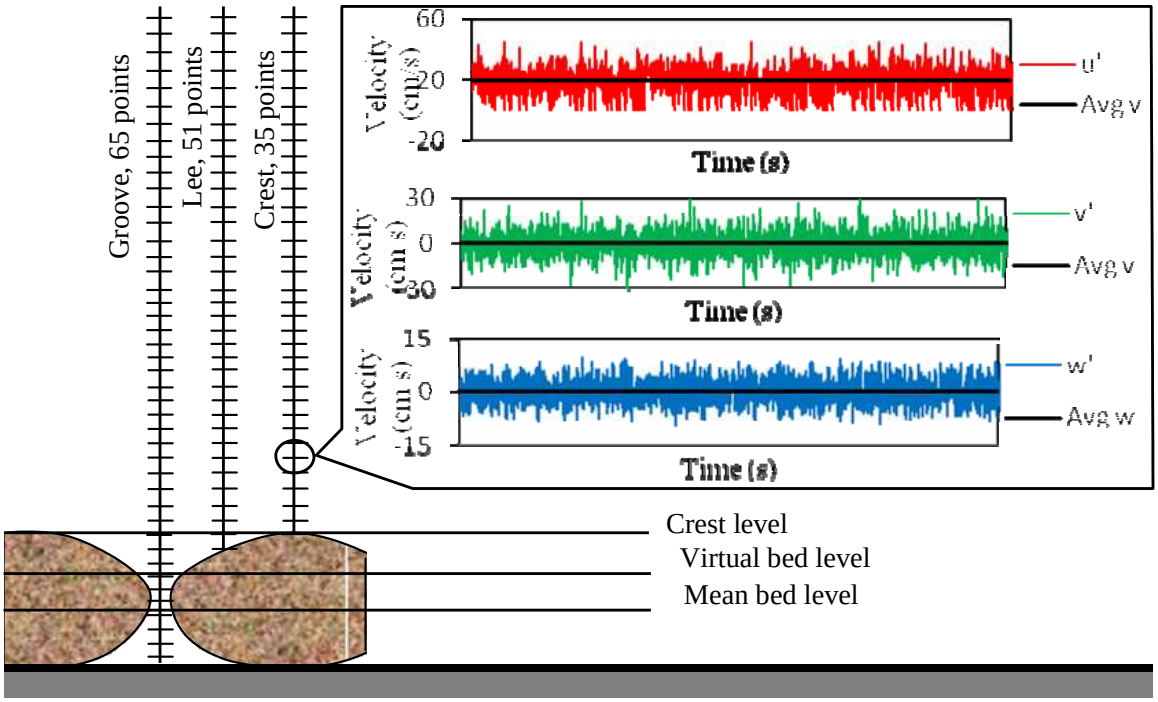


**Figure 3.** Locations of captured ADV Data.

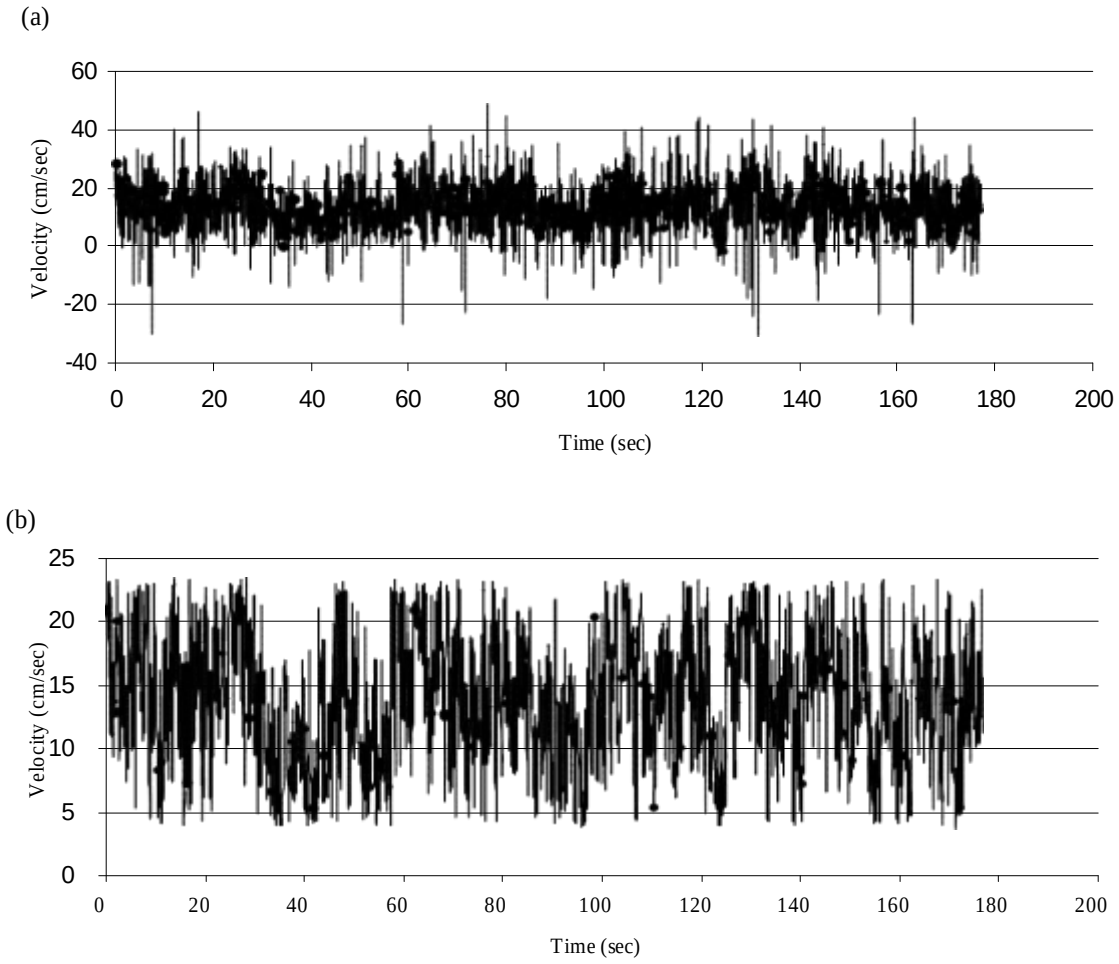


**Figure 4.** Vectrino data (a) before spike removal (b) after spike removal.

and error) in such a way so that the velocity power spectra provided an acceptable fit with Kolmogorov "–5/3 scaling-law" in the inertial subrange (Lacey and Roy, 2008) as shown in Figure 5.

## TURBULENT FLOW CHARACTERISTICS

### Stream-wise velocity distributions

Figure 6(a) illustrates the vertical distribution of stream-wise velocity, u with depth z above and below the groove. In the carrier fluid it is noted that, above the crest where the flow is not influenced by roughness element the profile is logarithmic. Below the crest level and within the groove velocity profile deviates from the logarithmic profile due to the direct influence gravel shape and compactness which necessitated the consideration of roughness geometry functions for examining the velocity profile below the crest. The velocity decreases to zero near the virtual bed level and further to negative values and thereafter increases to zero near the mean bed level. This is evident to the presence of rotational flows below the virtual bed level in the grooves. Figure 6(b) shows the vertical profile of the normalized stream-wise velocity $\tilde{u}$ in the groove. To fit the data plots within the wall-shear layer ($z > 0$) above the gravel crests to a logarithmic law (log law), $\overline{u}$ and $z$ are scaled by $u_*$ and $\Delta z$, respectively, such that $u^+ = \overline{u}/u_*$ and $z^+ = (z + \Delta z)/\Delta z$, where Δz = Nikuradse zero-plane displacement. To plot the experimental data, the log law is considered, as expressed in the following form:

$$u^+ = \frac{1}{\kappa}\ln\left(z^+\right) \quad (2)$$

Where κ = Von Karman coefficient. To plot the data $u^+\left(z^+\right)$ [Figure 6(a)], Δz is taken as $0.25d_{50}$ and κ as 0.41. The value of $u_*$ is obtained from $\tau_{uw}$ profile. The

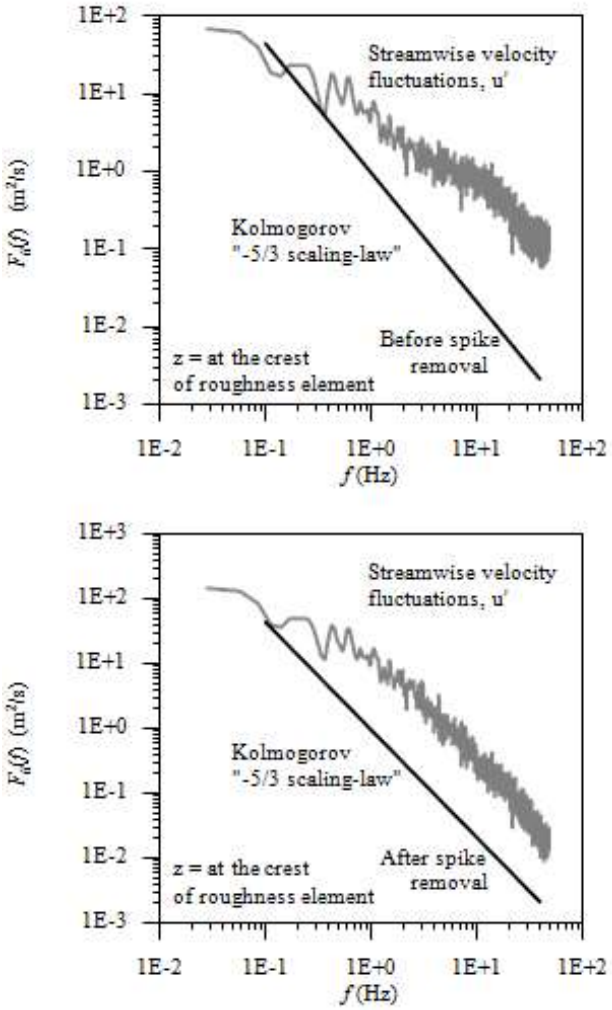


**Figure 5.** Spectral of streamwise velocity fluctuations (a) before spike removal (b) after spike removal.

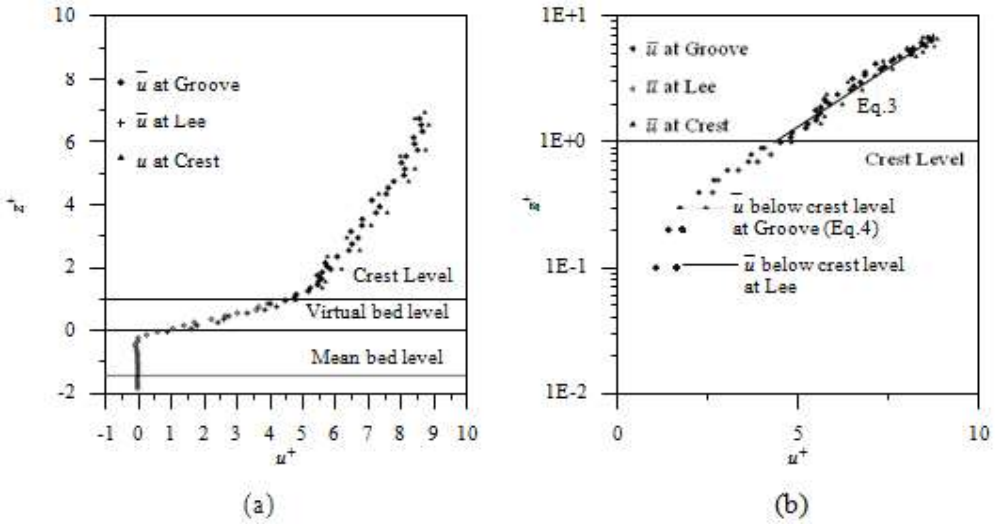


**Figure 6.** Streamwise velocity $u^+$ with normalized vertical distance $z^+$ in the Groove, Lee and above crest level considering roughness geometry function (φ).

**Table 1.** Bed shear stress, $\tau_b$ and shear velocity, $u_*$ obtained from $\tau_{uw}$.

| Location | $\tau_b$ | $u_*$ (cm/s) |
|---|---|---|
| Crest | 9.5 | 3.08 |
| Groove | 9.2 | 3.03 |
| Lee | 9.5 | 3.08 |

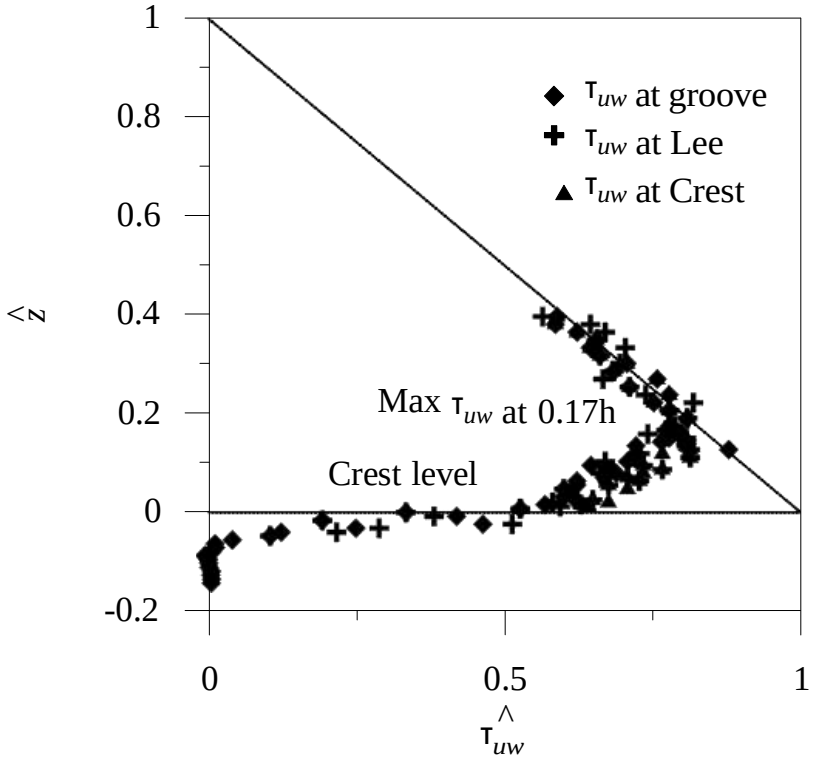


**Figure 7.** Variation of Normalised Reynolds shear stress $\tau_{uv}$ with flow depth.

log law for $u^+$ within the wall-shear layer above the gravel crests ($z^+$ > 1) is therefore given by:

$$u^+ = 2.439 \ln z^+ + 4.325 \quad (3)$$

On the other hand, the profile $u^+$ within the interfacial sub layer ($z^+ \leq 1$) fairly matches with a third-degree polynomial series given by:

$$u^+ = 2.0367 + 10.343 z^+ + 5.3019 z^{+2} - 4.3504 z^{+3} \quad (4)$$

It is in conformity with Dey and Das (2012) that the flows above the gravel crests ($z^+$ > 1) and within the interfacial sub layer ($z^+ \leq 1$) correspond to the log and the polynomial law, respectively.

**Reynolds shear stress distribution**

Reynolds shear stresses commonly termed as turbulent shear stress, $\tau_{uw}$ offers an appropriate tool for evaluating bed shear stress $\tau_0$ and subsequently the shear velocity $u_*$ (Nezu and Nakagawa, 1993) (Tables 1 and 2). Vertical distribution of Reynolds shear stress $-(\overline{u'w'})$ in the present study is plotted in Figure 7. In the wall region, the Reynolds stress attains a maximum value and decreases towards the bed. Similar results have been reported in other studies with rough beds (Grass, 1971). In the case of smooth walls this behaviour is due to viscous effects, while for rough walls it can be explained by the existence of a roughness sub-layer where additional mechanisms for momentum extraction emerge. From the plots of Reynolds shear stresses it is observed

**Table 2.** Experimental parameters.

| $S_0$ (%) | $Q$ (l/s) | $d_{50}$ (m) | $k_S$ | $h_0$(m) | A(m$^2$) | $R$(m) | $R_e$ | $U$(m/s) | $u_*$(m/s) | $R_*$ | $F_r$ | $z_c$(m) |
|---|---|---|---|---|---|---|---|---|---|---|---|---|
| 0.1 | 14 | 0.04 | 35.91 | 0.14 | 0.052 | 0.076 | 22442.7 | 0.210 | 0.030 | 916.030 | 0.179 | 0.01 |

Hydraulic parameters: $S_0$ channel slope, Q discharge, $d_{50}$ mean diameter of the particle, ks roughness coefficient, $h_0$ water depth (measured as distance between mean bed level and the water surface), A cross sectional area of flow, R =A/P hydraulic mean depth, Re =Uh/v Reynolds number, U average observed velocity, $u_*$ friction velocity, R* shear Reynolds number, Fr = $U/(gh)$Froude number, $z_c$ sediment crest level from the virtual bed level ($0.25d_{50}$).

**Table 3.** Bed shear and shear velocity.

| From slope | | From RSS | | From Clauser method | |
|---|---|---|---|---|---|
| $u_*$ (m/s) | $\tau_{slope}$ | $u_*$ (m/s) | $\tau_{RSS}$ | $u_*$ (m/s) | $\tau_b$ |
| 0.029 | 0.00084 | 0.03 | 0.00092 | 0.0238 | 0.000567 |

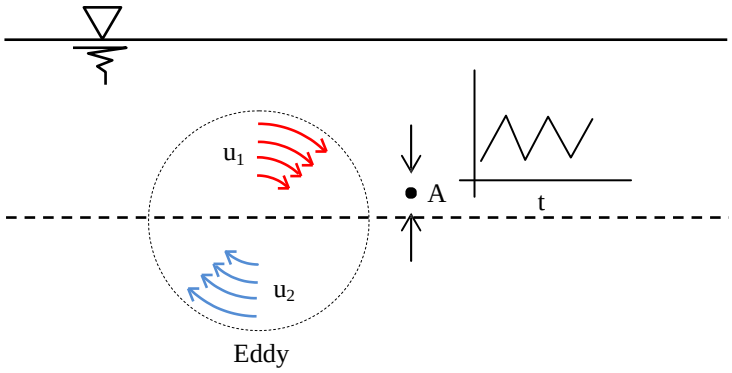


**Figure 8.** Schematic of eddy movement.

that the shear stress attains a maximum value just above the crest level and then decreases linearly with distance from the bed. A line drawn from the water surface through the maximum shear stress makes an intercept at the crest level which is equal to the bed shear stress, $\tau_0$ and collapse on the gravity line. Bed shear stress and hence the shear velocity $u_*$ are also estimated from (a) bed slope and (b) closure method using Colebrook-White equation and the values are summarized in Table 3.

## Power spectral density

In turbulent flows eddies are responsible to cause high fluctuations in the adjacent flow layers. Considering a point A as shown in Figure 8 in a fully turbulent flow region which is affected by eddies and bringing fluid particles of velocities $u_1$ and $u_2$ to A. Thus the velocity fluctuations at a point is descriptive of eddies that pass through that point. Close observations of velocity fluctuations reveal the presence of various sizes of eddies. Figure 9 shows the velocity fluctuations due to eddies and the resultant eddy size in the inertial subrange can be expressed by Taylor microscale $\lambda_T$ as given as:

$$\lambda_T = \left( \frac{15\upsilon \overline{u'u'}}{\varepsilon} \right)^{0.5} \quad (5)$$

where $\varepsilon$ = TKE dissipation rate and can be determined from the Kolmogorov's second hypothesis by calculating the following factors (Pope, 2001):

$$k_w^{5/3} S_{uu} = C\varepsilon^{2/3} \quad (6)$$

where $k_w$ = wave number; $S_{uu}(k_w)$ = spectral density function for $u'$; and $C$ = constant, being approximately 0.5 (Monin and Yaglom, 2007). A typical spectrum $S_{uu}(k_w)$ [= $(0.5\bar{u}/\pi)F_{uu}(f)$] versus $k_w$ [= $(2\pi/\bar{u})f$] at the crest level by filtering the instantaneous $u$ data is shown in Figure 10.

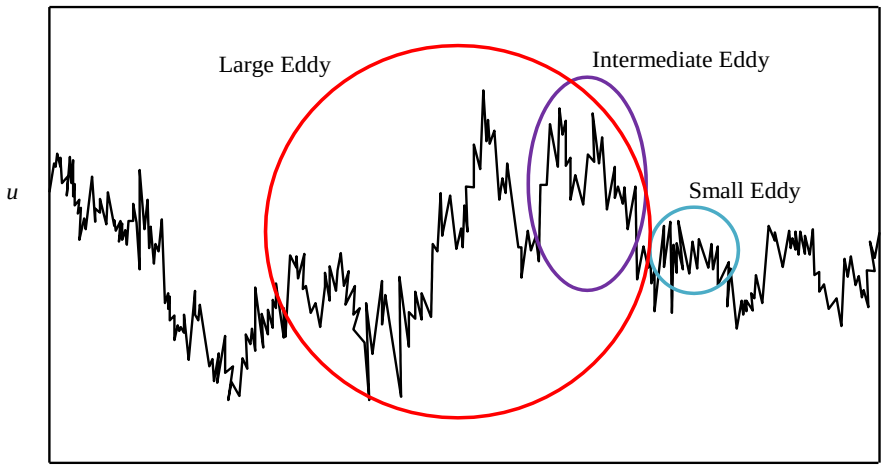


**Figure 9.** Velocity fluctuations due to eddies.

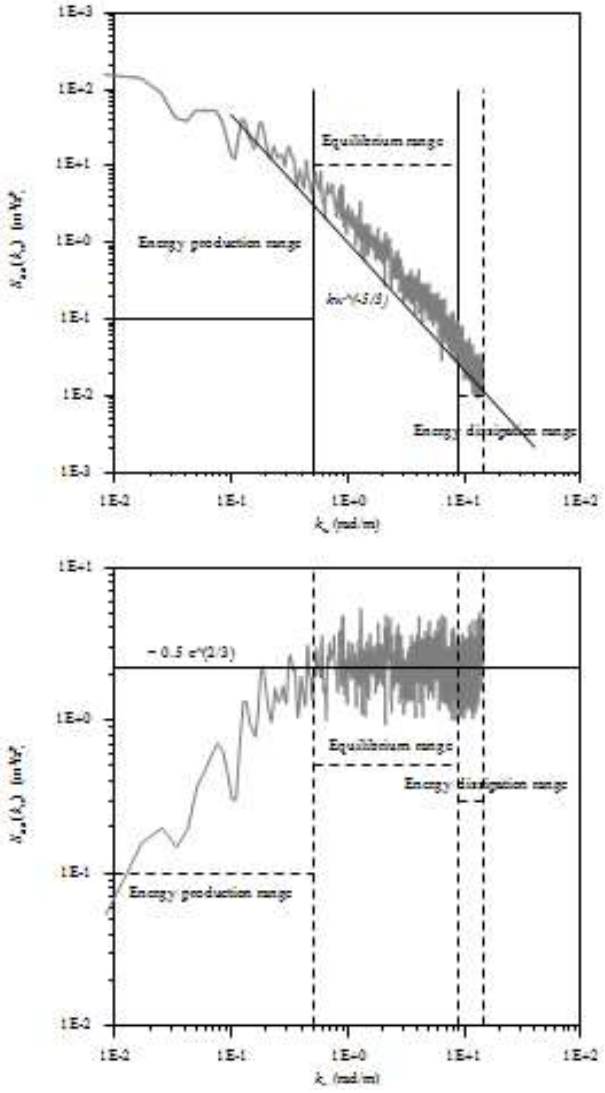


**Figure 10.** Velocity power spectra $S_{uu}(k_W)$ and turbulent dissipation rate ε at crest level.

**Table 4.** Frequency of various sub-ranges.

| Location | Distance from crest level (cm) | Frequency (Hz) | | |
|---|---|---|---|---|
| | | Energy production range | Slope of Equilibrium range (-5/3) | Dissipation range |
| Crest | 0 | 0.03 – 5.5 | 18 - 27 | 27 - 50 |
| $RSS_{max}$ | 1.5 | 0.03 – 7.6 | 22 - 30 | 30 - 50 |
| In the main Flow region | 3.3 | 0.03 – 4.6 | 20 - 30 | 30 - 50 |

In the inertial subrange the observed data showed conformity with Kolmogorov "–5/3 scaling-law". Then the dissipation rate, $\varepsilon$ is determined from Equation 6, and $\lambda_T$ from Equation 5. In the present study the spectral data is extensively investigated also at various depth levels and summarized in Table 4. No significant variations is observed but a three-range model of spectra has been noted which consists of: (1) the production range where spectral behaviour has not been identified specifically; (2) the inertial sub range where spectra follow the "-5/3" law; and (3) the viscous range where spectral density decays much faster than in the inertial sub range and the frequencies of each sub ranges are summarized in Table 4.

## Conclusions

The turbulent characteristics over rough bed were studied experimentally. Time averaged stream-wise velocity, Reynolds shear stresses, bed shear stress and statistical analysis of velocity fluctuations were studied and some important findings are summarized as follows:

(i) The velocity distribution in the outer layer was similar to that for flows over hydraulically smooth beds as stated by Nezu and Nakagawa (1993).
(ii) In the region below the crest level the velocity profile deviated from the logarithmic profile due to the direct influence of the roughness elements.
(iii) The velocity decreased to zero near the virtual bed level and further to negative values and thereafter increased to zero near the mean bed level. This is evident to the presence of rotational flows below the virtual bed level in the grooves.
(iv) Reynolds shear stress attains a maximum value just above the crest level and then decreases linearly with distance from the bed. A line drawn from the water surface through the maximum shear stress makes an intercept at the crest level which is equal to the bed shear stress.
(v) The spectral data showed no significant deviations at different horizontal locations. The spectral data was analyzed at various vertical distances and three clear sub-ranges were identified.

## Notation

$C$ = constant used for estimation of $\varepsilon$ (–);
$d_{50}$ = median size of gravels (m);
$k_w$ = wave number ($m^{-1}$);
$Q$ = water discharge ($m^3s^{-1}$);
$Re$ = flow Reynolds number, $4hU/\upsilon$ (–);
$Re_*$ = shear-particle Reynolds number (–);
$S$ = streamwise bed slope (–);
$S_{uu}$ = spectral density as a function of $k_w$ ($m^3s^{-2}$);
$U$ = depth-averaged flow velocity ($ms^{-1}$);
$\bar{u}$ = time-averaged streamwise velocity ($ms^{-1}$);
$u'$ = fluctuations of streamwise velocity ($ms^{-1}$);
$u^+$ = nondimensional streamwise velocity, $\bar{u}/u_*$ (–);
$u_*$ = shear velocity ($ms^{-1}$);
$u_i$ = Discrete velocity time series (s);
$w'$ = fluctuations of vertical velocity ($ms^{-1}$);
$z$ = elevation with respect to the roughness crest level (m);
$z^+$ = nondimensional vertical distance, $(z + \Delta z)/\Delta z$ (–);
$z_c$ = crest level of gravel or top of interfacial sublayer (m);
$\hat{z}$ = $z/h$ (–);
$\Delta z$ = depth of the virtual bed level from the bed surface (m);
$\Delta z$ = Nikuradse zero-plane displacement (m);
$\varepsilon$ = roughness thickness (m);
$\phi$ = roughness geometry function (–);
$\kappa$ = von Kármán coefficient (–);
$\lambda_u$ = Universal threshold (–);
$\lambda_T$ = Taylor microscale (m);
$\rho$ = mass density of fluid ($kgm^{-3}$);
$\tau$ = Reynolds shear stress, $-\rho\overline{u'w'}$ ($kgm^{-1}s^{-2}$);
$\tau_{uw}$ = Reynolds shear stress, $-\rho\overline{u'w'}$ ($kgm^{-1}s^{-2}$);
$\hat{\tau}_{uw}$ = nondimensional RSS (–);
$\tau_0$ = bed shear stress, $\rho u_*^2$ ($kgm^{-1}s^{-2}$);
$\upsilon$ = kinematic viscosity of fluid ($m^2s^{-1}$).

## CONFLICT OF INTERESTS

The authors have not declared any conflict of interests.

### REFERENCES

Grass AJ (1971). Structural features of turbulent flow over smooth and

rough boundaries. Journal of Fluid Mechanics 50(2):233-255.
Dey S, Das R (2012). Gravel-bed hydrodynamics: A double averaging approach. Journal of Hydraulic Engineering,ASCE 138(8):707-725.
Franca MJ, Ferreira RML, Lemmin U (2008). Parameterization of the logarithmic layer of double-averaged stream-wise velocity profiles in gravel-bed river flows. Advanced Water Resources 31:915-925.
Goring DG, Nikora VI (2002). Despiking acoustic Doppler velocimeter data. Journal of Hydraulic Engineering,ASCE 128(1):117-126.
Ibrahim MM, Abdel-Mageed NB (2014). Effect of bed roughness on flow characteristics. International Journal of Academic Research Part A, 6(5):169-178.
Lacey RWJ, Roy AG (2008). Fine-scale characterization of the turbulent shear layer of an in stream pebble cluster. Journal of Hydraulic Engineering ASCE 134(7):925-936.
Manes C, Pokrajac D, McEwan I (2007). Double-averaged open-channel flows with small relative submergence. Journal of Hydraulic Engineering ASCE 133(8):896-904.
Mignot E, Barthelemy E, Hurther D (2009a). Double-averaging analysis and local flow characterization of near-bed turbulence in gravel-bed channel flows. Journal of Fluid Mechanics 618:279-303.
Monin AS, Yaglom AM (2007). Statistical fluid mechanics, volume II: Mechanics of turbulence. Dover Publications, New York, USA.
Nezu I, Nakagawa H (1993). Turbulence in open-channel flows. Balkema, Rotterdam, Netherlands.
Nikora VI, Goring DG, Biggs BJF (2002). On gravel-bed roughness characterization. Water Resources Research 34(3):517-527.
Nikora V, Goring D, McEwan I, Griffiths G (2001). Spatially averaged open-channel flow over rough bed. Journal of Hydraulic Engineering ASCE 127(2):123-133.
Nikora V, Rowiński PM (2008). Rough-bed flows in geophysical, environmental and engineering systems: Double averaging approach and its applications. Acta Geophysica Special Issue 56(3):529-934.
Pal D, Ghoshal K (2014). Effect of bed roughness on grain-size distribution in an open channel flow. Journal of Hydro-environment Research 8(4):441-451.
Pokrajac D, Campbell LJ, Nikora V, McEwan IK, Manes C (2007). Quadrant analysis of persistent spatial velocity perturbations over square-bar roughness. Experiment of Fluids 42(3):413-423.
Pope SB (2001). Turbulent flows. Cambridge University Press, U.K.
Reidenbach MA, Limm M, Hondzo M, Stacey MT (2010). Effects of bed roughness on boundary layer mixing and mass flux across the sediment-water interface. Water Resources Researches 46(7):1-15.
Sadeque MA, Rajaratnam N, Loewen MR (2009). Effects of Bed Roughness on Flow around Bed-Mounted Cylinders in Open Channels. Journal of Engineering Mechanics, ASCE 135(2):100-110.
Sarkar S, Dey S (2010). Double-averaging turbulence characteristics in flows over a gravel-bed. Journal of Hydraulic Research 48(6):801-809.